PASJ: Publ. Astron. Soc. Japan **999**, 999–9 (2000)

Low Iron Upper Limits in X-Ray Afterglow of Two Gamma-Ray Bursts with ASCA

Daisuke Yonetoku,* Toshio Murakami, Yoshihiro Ueda, and Manabu Ishida
ISAS, 3-1-1, Yoshinodai, Sagamihara, Kanagawa 229-8510
E-mail(DY): yonetoku@astro.isas.ac.jp
Atsumasa Yoshida, Naoyuki Kawai, and Yuji Shirasaki
The Institute of Physical and Chemical Research, 2-1, hirosawa, Wako, Saitama 351-0198
and
Shin'ichiro Uno
Nihon Fukushi University Faculty of Social and Information Sciences, 26-2, Higashihaemi-cho Handa, Aichi 475-0012

(Received 1999 ; accepted 1999)

Abstract

An iron emission line in X-ray afterglow spectrum of Gamma-Ray Burst is thought to be an important key to understand the environment of a progenitor. The previous two observations of BeppoSAX and ASCA reported independently a strong red-shifted iron emission line. However both results were not firmly established statistically. The Japanese X-ray satellite ASCA observed two additional X-ray afterglows of GRB 990123 and GRB 990704 in 1999. The new spectra can be explained by a simple power-law with an excess absorption but without any iron feature. A 90% upper limit for the iron line flux is as low as $F_{\rm Fe} = 3.3 \times 10^{-6}$ photons cm^{-2} s^{-1} or less than 99.6 eV in equivalent width (EW). This upper limit is an order of lower than the previous two values of 1-3 keV in EW. We discuss this low upper limit in the frame work of Hypernova driven fireball.

Key words: Gamma-ray: burst, hypernova, neutron star

1. Introduction

Gamma-Ray Bursts (hereafter call GRBs) are the most energetic phenomena in the universe with a total energy of almost 10^{50-52} ergs, if beamed (Kulkarni et al. 1999). Although standard fireball models (Rees et al. 1922, Piran 1998) can explain many observational properties of GRBs in radio through X-ray and Gamma-ray, a true central engine of GRBs are still hidden. One of the most important keys, to make clear the unknown central engine and an environment of the progenitor, is the iron emission line associated with X-ray afterglows. There are several theoretical predictions for the iron line, but the intensity depends on the two competing scenarios for the origin of the iron line. One is a so-called clean fireball and the other is a dirty fireball (Mészáros et al. 1992,Paczyński 1997). The strong iron emission can be produced only in the iron rich dirty environment such as in the star forming regions, but a binary neutron star merger, mostly at outside the galactic disk, will not be able to produce a strong iron emission in such a clean environment. If the strong iron emission is confirmed, we may be able to answer the site of GRBs and also a probable environment.

In the past, strong iron emission lines were reported independently by the Advanced Satellite for Cosmology and Astrophysics (ASCA) in the spectrum of GRB 970828 (Yoshida et al. 1999) and in the spectrum of GRB 970508 by BeppoSAX (Piro et al. 1999). GRB 970828 was detected by the All Sky Monitor (ASM) onboard the Rossi X-ray Timing Explorer (RXTE) on August 28.73931, 1997 UT. The GRB was quickly localized to a position of R.A. = $18^{\rm h}08^{\rm m}32\overset{\rm s}{.}2$ and Dec. = $+59^\circ18'54''$ in 2000 coordinates with a 90 % error radius of $0\overset{'}{.}5$. ASCA monitored the X-ray afterglow during the period of August 29.91 - 30.85 UT (Murakami et al. 1999). The observed X-ray flux in band was $F_X = 4 \times 10^{-13}$ ergs cm^{-2}s^{-1} in 2.0 - 10 keV. And there was a spectral feature at $5.04^{+0.23}_{-0.31}$ keV in the spectrum. Assuming a power-law spectrum for this, ~ 3 keV in EW or the flux of $F_{\rm Fe} = (1.5 \pm 0.8) \times 10^{-13}$ ergs cm^{-2}s^{-1} was reported (Yoshida et al. 1999). The line feature was rather broaden to $\sigma = 0.31^{+0.38}_{-0.31}$ keV. However the F-test for the line was slightly less than three sigmas (99.4%).

* Department of Physics, Tokyo Institute of Technology, 2-12-1 Ookayama, Meguro, Tokyo 152-0033

The 5.04 keV line energy suggested a distance of a red-shift of $z = 0.33$. In addition to the iron line, an excess absorption, which could not be explained by our galactic column density, was also reported (Yoshida et al. 1999). The excess value was $N_{\mathrm{H}} = 4.1 \times 10^{21}$ cm^{-2} at the rest frame of z = 0.33. However the Very Large Array (VLA) in radio band discovered a flare coincided with the X-ray afterglow (Frail D. 1999 private communication). Keck observation of the position discovered a galaxy and measured a different red-shift of z = 0.96 for the galaxy. ! ! This distance is inconsistent with the ASCA result of z = 0.33 (George D. private communication 1999).

Independent to the ASCA report, the iron emission line from GRB 970508 was descovered by BeppwSAX. The red-shift distance of 0.835 was measured from the Optical Transient (OT) (Bloom et al. 1998). The X-ray afterglow was monitored for 6 hours and the iron line with $I_{\mathrm{Fe}} = (5\pm2)\times10^{-5}$ photons cm^{-2}s^{-1} or equivalently $\sim$ 1 keV in EW was reported by BeppoSAX (Piro et al. 1999). Although the red-shift decided from the iron line was consistent with the OT distance, the F-test was also slightly less than three sigma confidence level in this case (Piro et al. 1999). ! ! ! These iron features have not become a strong evidence of dirty environment yet.

Although the discoveries of a strong iron line were reported independently by BeppoSAX and ASCA, two difficulties can be pointed out for the results beside the inconsistent red-shift value between ASCA and Keck. First, both results showed less than three sigma confidence level in the F-test for an additional one parameter of the iron line structure. Second, both line features were seen only in some specific intervals which may be associated with a flare like activity and then the iron intensities were very variable. Clearly, we require further observations with a better S/N for establishing the iron line feature. Thus, ASCA observed two additional X-ray afterglows of GRBs to confirm the iron line emission.

2. Observations and Data Reduction

ASCA Target of Opportunity Observations of the two X-ray afterglows of GRB 990123 and GRB 990704 were done following the BeppoSAX detection and two wide band X-ray spectra were obtained by the Gas Imaging Spectrometers (GIS) and by the Solid-state Imaging Spectrometers (SIS) (Tanaka et al. 1994). The SIS was set to 1 CCD faint mode and the GIS was set to PH mode. The analysis of the data was done based on the standard procedure of ASCA. Most case, intensities of X-ray afterglow was weak at one day after the burst and no brighter than the typical background level. So we selected the data and subtracted the background very carefully.

2.1. GRB 990123 light-curve

GRB 990123 was detected by BeppoSAX on January 23.408 UT and was located to the position of $\alpha = 231.3764$ and $\delta = 44.7664$ in 2000 coordinates (Piro 1999). The ground based optical observations discovered an OT associated with the GRB (Odewahn et al. 1999, Akerlof et al. 1999). Remarkably and surprisingly enough, this burst was also detected as a 8.95 magniture optical flash by ROTSE simultaneously with the burst (Akerlof et al. 1999). The Keck observation revealed a red-shift distance of 1.60 (Kelson et al. 1999) and HST detected a probable merging two galaxies (Bloom et al. 1999) at the OT position a manth later. The HST image suggests an association of the GRB to the star forming region (Bloom et al. 1999). The X-ray flux was 8.2×10^{-8} ergs cm^{-2}s^{-1} (3.4 Crab) in 1.5-20 keV range, and time duration was $\sim$ 100 s (Piro 1999).

ASCA started observation with a delay of $\sim$ 57.4 hours and monitored the afterglow for 80 ks from January 25.69 (UT) until 26.62 (UT) (Murakami et al. 1999). In the field of view of the GIS detector, there were a few nearby X-ray sources. We had to take care of these X-ray sources to subtract background to have a reliable data. The intensity of the flux decayed during the observation which is consistent with the power-law in time. The total exposure time was divided into three parts as shown in figure 1. The decay of -1.44 in power is consistent with the standard temporal behavior of the other afterglows. The X-ray flux averaged over the these periods is 6.15×10^{-13} ergs cm^{-2}s^{-1}. There was no flare like activity, which was observed in GRB 970828 and GRB 990508. The ASCA light curve of the afterglow is shown in figure 1.

2.2. GRB 990704 light-curve

The ASCA observation of GRB 990704, following the detection by BeppoSAX (Piro et al. 1999), started 16 hours after the burst and monitored the afterglow for 65 ks from July 4.36 (UT) until 5.02. The burst position was $\alpha = 184.79$ and $\delta = -3.80$ in 2000 coordinates (Murakami et al. 1999). Follow-up optical observations discovered an OT (Alain 1999) but the red-shift is unknown. The X-ray flux was bright of 1.5×10^{-7} ergs c^{-2}s^{-1} (6.2 Crab) in 2.0-10 keV during the burst, and the time duration was $\sim$ 40 s. GRB 990704 was much brighter than GRB 990123, but due to the fast decay in time, the mean flux at the time of the ASCA observation was a half of GRB 990123. There was no nearby X-ray source in the GIS field of view, so we chose the background region where the X-ray afterglow is in point symmetry to the optical axis of the ASCA X-ray mirrors. The light curve after subtracting the background is shown in figure 2.

Fig. 1. GIS X-ray light curve of GRB 990123 after subtracting a background in 2 - 10 keV. The X-ray flux of the BeppoSAX WFC averaged over the burst is also plotted in the same figure. The flux decreased with a power-law in time.

Fig. 2. The same as figure 1. but for GRB 990704. The ASCA window is divided into two intervals. The X-ray flux during the burst by the BeppoSAX WFC is also plotted in the same figure.

2.3. GRB990123 spectrum

The ASCA spectrum was acceptably fitted by a single power-law with absorption, after that, to add a line Gaussian to models, the upper limit of iron flux was set. This spectrum is shown in figure 3.

Fig. 3. X-ray spectrum of GRB 990123 combined with the four ASCA detectors into one figure. The spectrum can be explained without any iron structure at z = 1.60. 90 % upper limit for the 6.4 keV line is 3.26×10^{-6} photons $\mathrm{cm^{-2}s^{-1}}$ or EW = 99.6 eV.

Using fixed value to our galactic column density $N_{\rm H} = 2.09 \times 10^{20}$ cm^{-2} (W3nH) with a single power-law model, there was residual in the low energy part and $\chi^2(\nu) = 90(81)$. The free fit for the absorption yielded a column density of $N_{\rm H} = (0.145^{+0.068}_{-0.062}) \times 10^{22}$ cm^{-2} (90 % error) which is larger than the galactic value with a reduced $\chi^2(\nu) = 79(80)$. The large reduction in χ^2 suggests a significant absorption in the low energy spectrum. If we attribute this excess absorption to the host galaxy at z = 1.6, $N_{\rm H} = (1.15^{+0.65}_{-0.60}) \times 10^{22}$ cm^{-2} is required for the frame at the host galaxy. This is high but can be explained by a column density looked through the galactic disk. The power-law photon index of -1.78 ± 0.11 was a typical of X-ray afterglow and the X-ray flux was $F_X = 9.05 \times 10^{-6}$ photons cm^{-2}s^{-1} or $F_X = 6.15 \times 10^{-13}$ ergs cm^{-2}s^{-1} in 2.0-10 keV.

Next, the iron line Gaussian which assumed line width $\sigma = 0$, $E_{\rm Fe} = 6.4$keV and $z = 1.6$ was added in spectra. The conclusion was that only the upper limit of iron flux can be set as 3.26×10^{-6} photons cm^{-2}s^{-1} or 1.29×10^{-14} ergs cm^{-2}s^{-1} or 99.6 eV in EW with 90 % error. $\Delta\chi^2$ for the additional one parameter for the line is ~ 0, so any significant lines were not required with the F-test.

2.4. GRB 990704 spectrum

A spectrum of GRB 990704 was fitted by a simple power-law with our galactic column density of $N_{\rm H} = 1.10 \times 10^{21}$ cm^{-2} (W3nH). The conclusion has already been acceptable in $\chi^2(\nu) = 72(70)$. Due to the poorer S/N than GRB 990123, we cannot find an excess ab-

Fig. 4. X-ray spectrum of GRB 990704. A single power-law with a galactic absorption can explain the spectrum without any iron feature.

sorption in this case. The power-law photon index of -1.71 ± 0.12 is a typical of X-ray afterglow. The X-ray flux is $F_X = 7.52 \times 10^{-5}$ photons cm^{-2}s^{-1} or $F_X = 5.18 \times 10^{-13}$ ergs cm^{-2}s^{-1} in 2.0-10.0 keV range. The red-shift to the burst is not known for this case, so we searched for a most realistic range of distances between 0.3 and 4 which were reported for the previous GRBs. The iron line at energy $E_{\rm Fe}$ of 3.0 ± 0.4 keV, which corresponds to $z = 1.14$ for the 6.4 keV iron, showed the best fit but the F-test again does not allow an additional one parameter. An upper limit to the iron line is set to be 4.67×10^{-6} photons cm^{-2}s^{-1} or 2.24×10^{-14} ergs cm^{-2}s^{-1} or 245 eV in EW.

3. Discussion

The ASCA observations of X-ray afterglow of GRB 990123 and GRB 990704 set an order of lower upper limits to the iron line intensity then before. Among two, the iron upper limit for GRB 990123 is less than 100 eV in EW or equivalently $F_{\rm Fe} = 1.3 \times 10^{-14}$ ergs cm^{-2}s^{-1} or 3.3×10^{-6}photonscm^{-2}s^{-1}. The new ASCA upper limit is an order of lower than the values of ~ 3 keV by ASCA in GRB 970828 and 1 keV in EW by BeppoSAX in GRB 970508. Using the new iron upper limit and the distance to GRB 990123, we can estimate a matter associated with the fireball or a matter surrounding the X-ray afterglow. Only the distance of GRB 990123 (Kelson et al. 1999) is known, so we focus into GRB 990123 in the following discussion.

The burst fluence of GRB 990123 was bright of 2.4×10^{-6} ergs cm^{-2} and roughly corresponds to 10^{54}, if not beamed and 10^{52} ergs, if beamed at z=1.60 (Kelson et al. 1999, Kulkarni et al. 1999). The change in the decay slope of the OT strongly suggests beaming for the burst (Kulkarni et al. 1999), so we use the value of 10^{52} ergs in the following discussion. A number of iron photons, required at z=1.6, is huge and is roughly 10^{55} photons from the iron flux of 5×10^{-5} photons cm^{-2}s^{-1}. Assuming a typical cosmological abundance $A_{\odot} \sim 1$ in solar unit and a fluorescent yield of $q \sim 0.1$, a mass lower limit to explain the above iron photons is estimated below.

$$M \geq 1.3 \times 10^{-2} \frac{F_{\rm Fe,14}\ t_5\ R_{16}^2}{q_{-1}\ A_{\odot}\ E_{52}}\ M_{\odot}\ {\rm g}, \qquad (1)$$

where t_5, is the time scale of the afterglow in unit of 10^5 s. Roughly 10^{-2} $M_{\odot}$ is required to explain the observed iron photons (Lazzati et al. 1999). It is very hard to explain this amount of matter by a typical matter surrounding a progenitor. Even if a progenitor is a high mass loss main-sequence giant with a stellar-wind in a pre-Hypernova phase, the wind cannot reach to the amount within the radius of 10^{16} cm in size (Lazzati et al. 1999).

If the observed excess in $N_{\rm H}$ in the low energy spectrum is entirely attributed to the circumstellar matter surrounding a progenitor, the hydrogen mass $M^{(\rm H)}$ surrounding the fireball can be estimated below

$$M_H = (4.0^{+1.4}_{-1.1} \times 10^{-3})\ R_{16}^2 M_{\odot}, \qquad (2)$$

where 10^{16} R_{16} cm is the length that light can cross during the observed delay. The mass has a possibility to explain the required mass of equation(1). However, there is no reason to think that the excess absorption is entirely from the circumstellar matter. More reasonably, it should be a gas associated with the host galactic disk.

A fireball theory with a relativistic Lorentz factor of several hundred (Rees et al. 1992), requires a low baryon loading. The loading is not expected to be more than 10^{-6} $M_{\odot}$ in mass for a GRB with a total energy of 10^{52} ergs (Rees et al. 1992). Thus, it is very hard to compromise the amount of material derived from the observed upper limit, with the theoretical requirement. If the observed values are true, the material for iron line emission should not be attributed to the fireball but rather to the dense surrounding. However, even the strong stellar wind in a giant phase cannot afford to explain such a large amount of material. The no optical and infra-red extinction except the case of GRB 980326 also cannot support a large amount of circumstellar matter around a progenitor (Groot et al. 1998). Many theoretical works predict a strong iron emission line associated with the X-ray afterglow, but we cannot have a firm detection of the iron. We only have two suggestive data and two low upper limits. Independently our works, BeppoSAX also searched for sixteen GRBs but non of them showed not only any iron line feature but also a flare activity (Piro 1999 private communication).

In conclusion, two of the bright GRBs were observed with ASCA and both did not show any iron line feature. A low upper limit of 100 eV in EW is set. This new upper limit is still high in point of view of mass but the low value should be considered in the theoretical works. To establish a firm detection or to have a much lower upper limit, we require more sensitive observations such as by XMM, Chandra and ASTRO-E, which have an order of excellent ability than the previous satellites.

Table 1. Model spectral parameters.

parameters	GRB990123	GRB990704
Γ	1.78 ± 0.11	1.71 ± 0.12
$F_X{}^*$ **(2-10 keV)**	6.15×10^{-13}	5.20×10^{-13}
$F_X{}^\dagger$ **(2-10 keV)**	9.05×10^{-5}	7.56×10^{-5}
$F_{\rm Fe}{}^*$	1.3×10^{-14}	2.5×10^{-14}
$F_{\rm Fe}{}^\dagger$	3.3×10^{-6}	5.1×10^{-6}
z	1.60	$\cdots$
$N_{\rm H}{}^\flat$	2.09×10^{20}	1.10×10^{21}
$N_{\rm H}{}^\sharp$	$(1.15^{+0.65}_{-0.60}) \times 10^{22}$	$\cdots$

$*$ ergs cm^{-2}s^{-1} (90 % upper limit).
$\dagger$ photons cm^{-2}s^{-1} (90 % upper limit).
$\flat$ cm^{-2} (our galactic column density).
$\sharp$ cm^{-2} estimated column density at z = 1.6).

References

Akerlof C. W., et al. 1999, Nature 398, 400-402

Akerlof C. W., and McKay T. A. 1999, Gamma-Ray Burst Coodinates Network (GCN) No.205

Alain M 1999, GCN No.363

Bloom, J.S., Djorgovski, S.G., Kulkarni, S. R. 1998, astro-ph/9807315

Bloom J. S., Odewahn S. C., Djorgovski S. G., Kulkarni S. R., Harrison F. A., Koresko C., Neugebauer G., and Armus L. et al 1999, ApJL, 518, L1

George private communication 1999, in Huntsbil

Groot P.J., Galama T. J., Vreeswijk P. M., Wijers R. A. M. J., Pian E., Palazzi E., van Paradijs J., and Kouveliotou C. et al. 1998, ApJL 502, L123

Kelson D. D., Illingworth G. D., Franx M., Magee D., and van Dokkun P. G. 1999, I.A.U.C. 7096

Kulkarni S. R., Frail D. A., Moriarty-Schieven G. H., Shepherd D. S., Udomprasert P. Readhead A. C. S., Bloom J. S., Feroci M., and Costa E. 1999, astro-ph/9903441

Lazzati D., Campana S., and Ghisellini G. 1999, MNRAS, 304, L31

Mészáros P. and Rees M.J., 1992, ApJ 397, 570

Murakami T., Yoshida A., Kawai N., Ishida M.. and Dotani T. 1999 GCN No.228

Murakami T., Yoshida A., Kawai N., Tamura T., Terada S., and Tsuru T. 1999 GCN No.372

Narayan R, Paczyński B, and Piran T 1992, astro-ph/9204001

Odewahn S. C., Bloom J. S., and Kulkarni S. R. 1999, GCN No.201

Owens A., Guainazzi M,. Oosterbroek T., Orr A., Parmar A.N., Costa E., Feroci M.GRB , Piro L., et al. 1999, A&A ***

Paczyński B. 1997, astro-ph/9706232

Piran T. 1999, Phys.Rept. 314, 575

Piro L., Costa E., Feroci M., Frontera F., Amati L., Fiume D Dal., Antonelli A., Heise J., et al. 1999, ApJL 514, L73

Piro L 1999, GCN No.199

Piro L 1999, GCN No.360

Rees M.J., Mészáros P. 1922, MNRAS, 258, L41

Tanaka Y, Inoue H, Holt S. S. 1994, PASJ, 46, L37

Yoshida A., et al. 1999, A&A 138, 433

Kulkarni et al. (1999?), Nature,

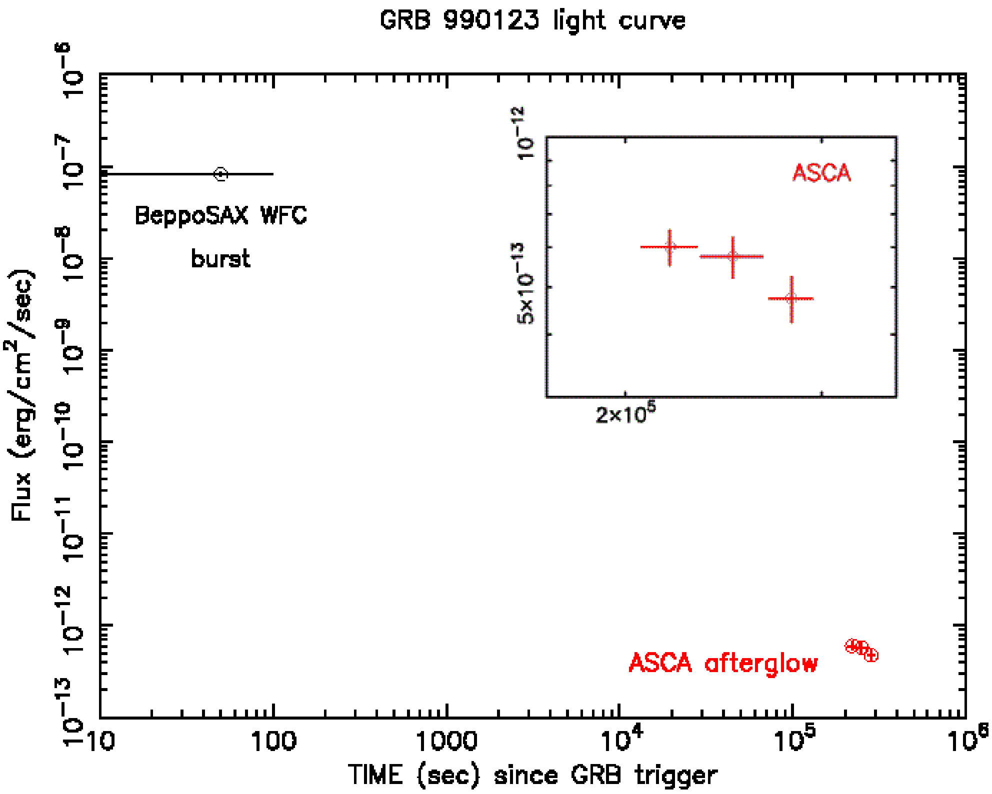
GRB 990123 light curve
Flux (erg/cm^2/sec)
10^{-6}
10^{-7}
10^{-8}
10^{-9}
10^{-10}
10^{-11}
10^{-12}
10^{-13}
BeppoSAX WFC
burst
ASCA
10^{-12}
5×10^{-13}
2×10^5
ASCA afterglow
10
100
1000
10^4
10^5
10^6
TIME (sec) since GRB trigger

Figure 1 :

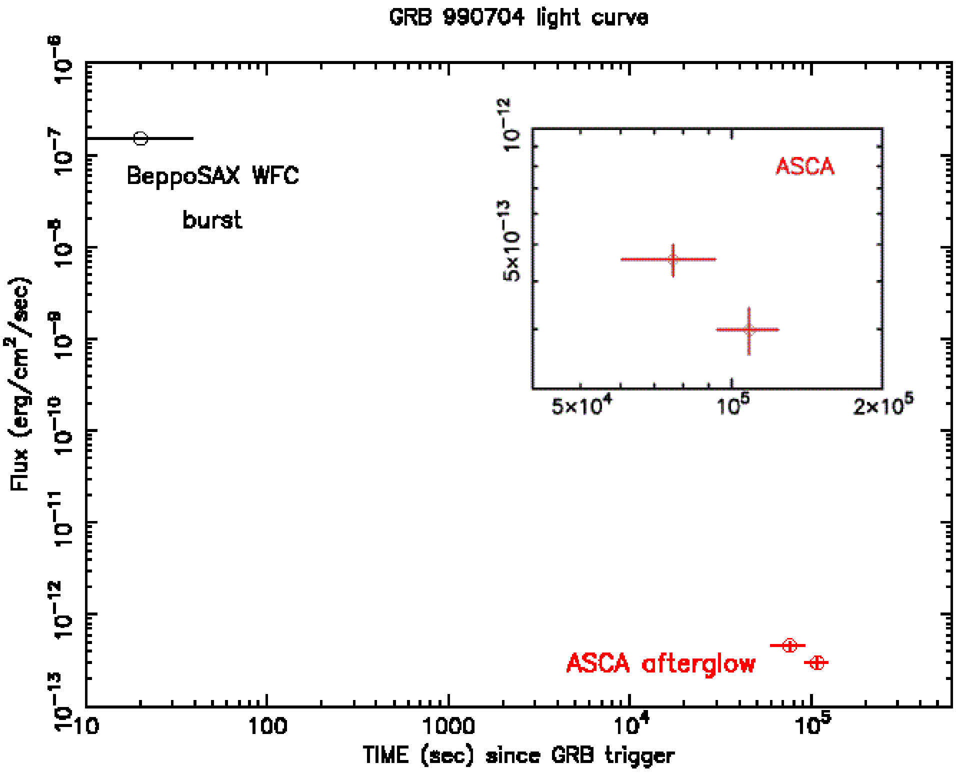

GRB 990704 light curve
Flux (erg/cm^2/sec)
TIME (sec) since GRB trigger
BeppoSAX WFC
burst
ASCA afterglow
ASCA
10^{-6}
10^{-7}
10^{-8}
10^{-9}
10^{-10}
10^{-11}
10^{-12}
10^{-13}
10
100
1000
10^4
10^5
10^{-12}
5×10^{-13}
5×10^4
10^5
2×10^5

Figure 2 :

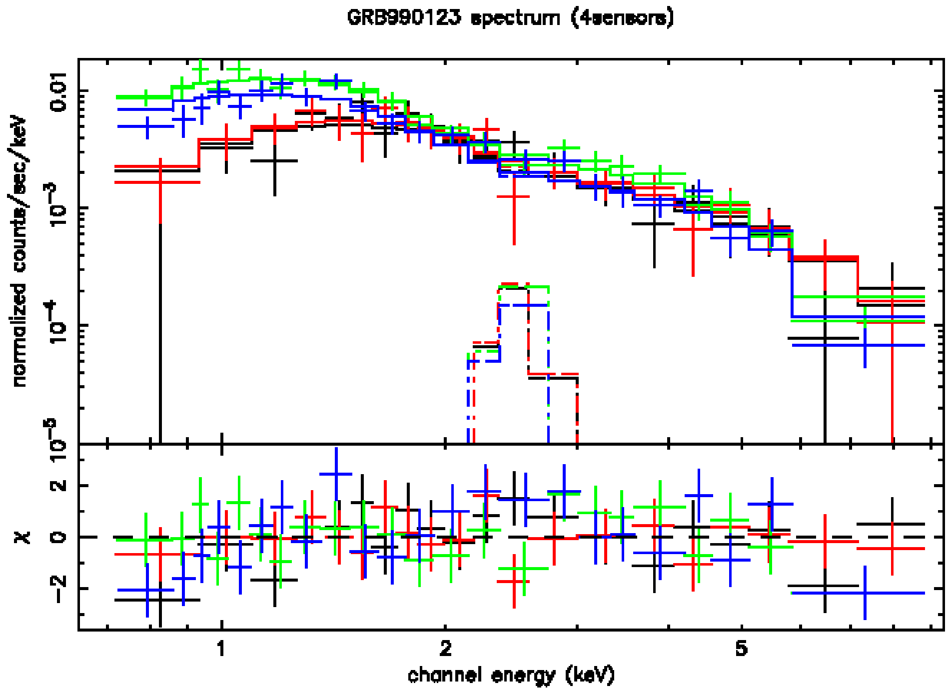
GRB990123 spectrum (4sensors)
normalized counts/sec/keV
0.01
10^{-3}
10^{-4}
10^{-5}
χ
2
0
−2
1
2
5
channel energy (keV)

Figure 3 :

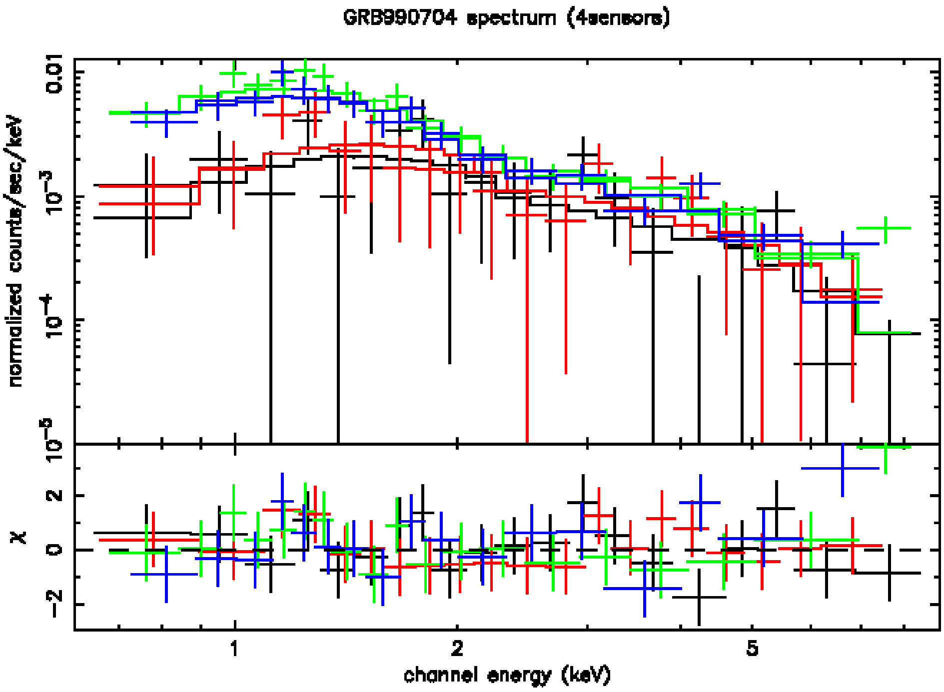
GRB990704 spectrum (4sensors)
normalized counts/sec/keV
0.01
10^{-3}
10^{-4}
10^{-5}
χ
2
0
−2
1
2
5
channel energy (keV)

Figure 4 :